PAPER

Biomarker-specific conjugated nanopolyplexes for the active coloring of stem-like cancer cells

To cite this article: Yoochan Hong *et al* 2016 *Nanotechnology* **27** 225101

IOP Publishing Nanotechnology
Nanotechnology 27 (2016) 225101 (8pp) doi:10.1088/0957-4484/27/22/225101

Biomarker-specific conjugated nanopolyplexes for the active coloring of stem-like cancer cells

Yoochan Hong[1,6], Eugene Lee[1,2,6], Jihye Choi[3], Seungjoo Haam[4,5], Jin-Suck Suh[1,5] and Jaemoon Yang[1,5]

[1] Department of Radiology, College of Medicine, Yonsei University, Seoul 03722, Korea
[2] Nanomedical National Core Research Center, Yonsei University, Seoul 03722, Korea
[3] Department of Radiation Oncology & Medical Physics, Stanford University, CA 94305, USA
[4] Department of Chemical and Biomolecular Engineering, Yonsei University, Seoul 120-749, Korea
[5] YUHS-KRIBB Medical Convergence Research Center, Yonsei University, Seoul 120-749, Korea

E-mail: 177hum@yuhs.ac

Received 13 November 2015, revised 15 March 2016
Accepted for publication 30 March 2016
Published 21 April 2016

Abstract

Stem-like cancer cells possess intrinsic features and their CD44 regulate redox balance in cancer cells to survive under stress conditions. Thus, we have fabricated biomarker-specific conjugated polyplexes using CD44-targetable hyaluronic acid and redox-sensible polyaniline based on a nanoemulsion method. For the most sensitive recognition of the cellular redox at a single nanoparticle scale, a nano-scattering spectrum imaging analyzer system was introduced. The conjugated polyplexes showed a specific targeting ability toward CD44-expressing cancer cells as well as a dramatic change in its color, which depended on the redox potential in the light-scattered images. Therefore, these polyaniline-based conjugated polyplexes as well as analytical processes that include light-scattering imaging and measurements of scattering spectra, clearly establish a systematic method for the detection and monitoring of cancer microenvironments.

S Online supplementary data available from stacks.iop.org/NANO/27/225101/mmedia

Keywords: polyaniline, hyaluronic acid, cancer, colorimetric probes, redox environment

(Some figures may appear in colour only in the online journal)

1. Introduction

The malignant features of cancer cells cannot be manifested without an important interplay between cancer cells and their local environment [1]. The tumor infiltrate, which is composed of immune cells, angiogenic vascular cells, lymphatic endothelial cells, and cancer-associated fibroblastic cells, contributes actively to cancer progression [2]. The ability to change these surroundings is an important property by which tumor cells are able to acquire some of the hallmark functions necessary for tumor growth and metastatic dissemination [3]. Thus, sensing of the tumor microenvironment for the destruction of cancer cells in their local environment has become important. From this awareness, many strategies and products based on nanotechnology have been proposed for clinical applications [4]. Some recent research showed that nanomaterial-enabled approaches were developed for cancer diagnosis via the recognition and targeting of specific components of the cancer microenvironment [5–7]. However, because the cancer microenvironment consists of various cell types and a complex extracellular matrix, it is extremely challenging to achieve specific and sensitive responses to a subtle stimulus, such as a molecular binding event or a specific trigger from local environmental changes [8].

Herein, we investigate the availability of conjugated polyaniline (PAni) nanoparticles for not only sensing of the cancer microenvironment but also for the recognition of a specific biomarker expressed on the cancer cells. The most

[6] These authors contributed equally to this work.

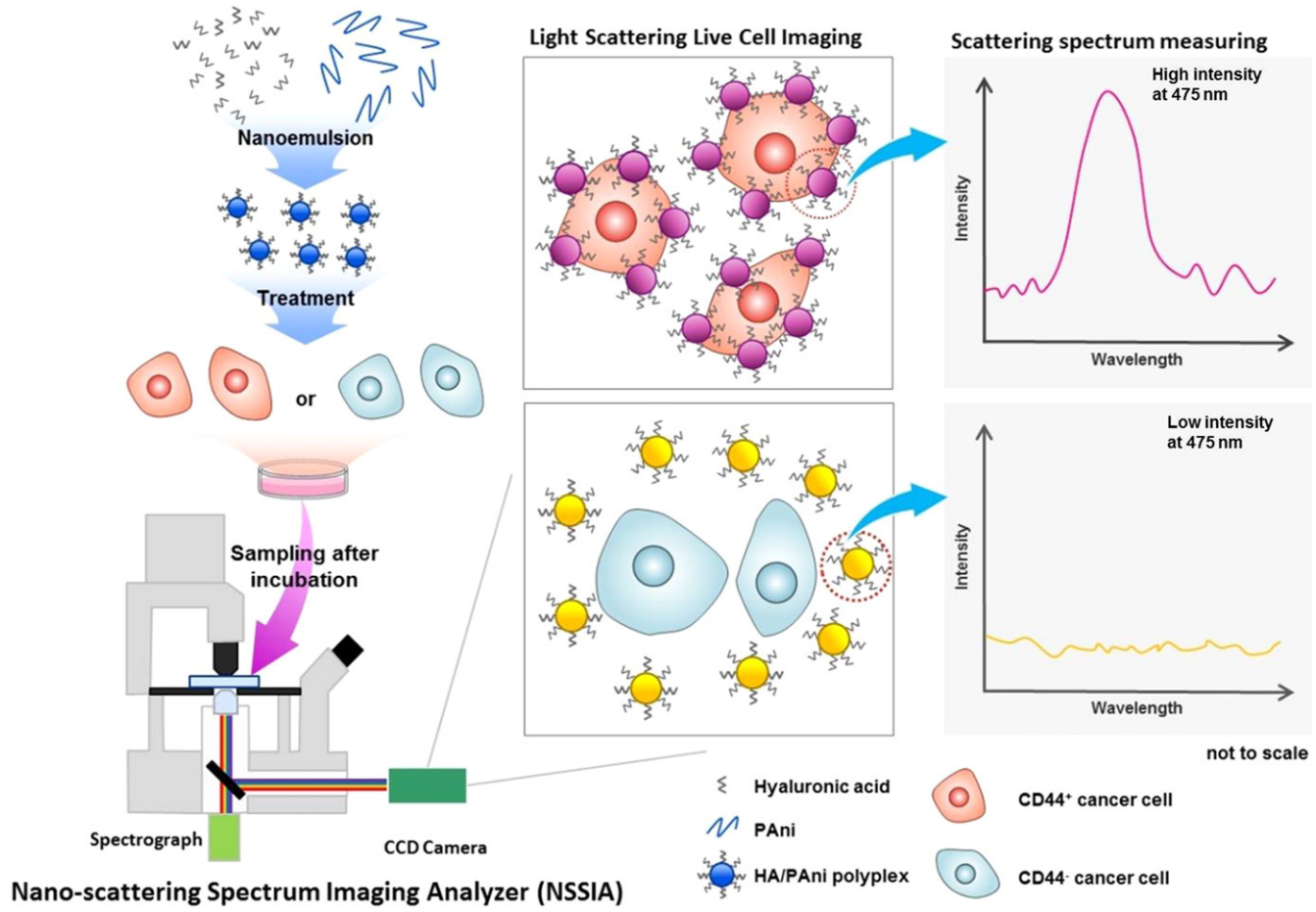

Figure 1. Schematic illustration of the preparation of active colorimetric probes based on polyaniline and their application for the sensing of malignant cancer cells using a nano-scattering spectrum imaging analyzer (NSSIA).

representative property of PAni is a doping mechanism that provides an interband gap state between valance and conduction bands to induce the movement of electrons and decreases excitation energy levels [9–11]. Consequently, the optical absorbance peak of PAni is red-shifted toward the long wavelength, and the state of polyaniline transitions from an emeraldine base (EB) into an emeraldine salt (ES). Therefore, the color of PAni visually changes from blue to green and from yellow to pink for darkfield microscopic images; thus, PAni nanoparticles can serve as colorimetric nanoprobes for cancer microenvironment sensing. Additionally, CD44, a cell surface glycoprotein that is overexpressed in breast cancer cells, plays an important role in promoting cancer cell proliferation, migration, invasion, and tumor-associated angiogenesis [12–14]. This biomarker is a major surface receptor for hyaluronic acid (HA), in particular, high-molecular weight HA (1 M Da), which can be used to fabricate polyplexes due to its polyanionic properties and targeting of CD44 [15, 16]. Therefore, HA-assemlbed PAni (HA/PAni) polyplexes were fabricated, and light-scattering imaging and spectral measurements of HA/PAni polyplexes or cancer cells with HA/PAni polyplexes were also performed for the sensitive detection of the cancer microenvironment as well as for the determination of CD44 expression levels (figure 1).

2. Materials and methods

2.1. Materials

Aniline, ammonium persulfate (APS), and Tween 80 were purchased from Sigma-Aldrich. Hydrochloric acid (HCl) and acetone were purchased from Daejung Chemical. Sodium hydroxide (NaOH) was purchased from Duksan Pure Chemicals. 1-methyl-2-pyrrolidone (NMP) was purchased from Samchun Pure Chemical. Hyaluronic acid (HA, M_w: 1 M) was obtained from Yuhan Pharmaceutical Corporation. Dulbecco's phosphate-buffered saline (PBS) was purchased from WelGENE Incorporated. Ultrapure deionized (DI) water was used for all synthetic processes. All other chemicals and reagents were of analytical grade.

2.2. Synthesis of polyaniline (EB)

The EB state of PAni was prepared by chemical oxidation polymerization using strong acid, such as HCl as described in previously published report with some modifications [7]. Briefly, 0.2 mole of aniline monomer was added into 300 ml of 1 M HCl. After that, 0.05 mole of APS solution in 200 ml of 1 M HCl was added via drop-wise method to the 300 ml of 1 M HCl solution containing aniline monomer for 6 h at 4 °C.

The resultant polymer salts were filtrated and re-dispersed in 500 ml of 0.2 M HCl solution, and these filtration and re-dispersion procedures were repeated twice. And then, the salts of precipitated polymer were repeatedly filtrated and re-dispersed in 500 ml of 1 M NaOH solution. Finally, PAni powder in EB state was obtained after filtration using 500 ml of acetone and dried in a vacuum oven for 48 h.

2.3. Preparation of hyaluronic acid polyaniline (HA/PAni) nanoparticles

For the preparation of HA/PAni nanoparticles, 5 mg EB powder was dispersed in 4 ml NMP. This organic phase was added to 30 ml DI water containing 100 mg HA. This mixture was vigorously stirred at room temperature for 24 h. After the reaction, HA/PAni nanoparticles were purified by dialysis for 24 h (M_w: 3500) and centrifugation for 4 h (3000 rpm). Absorbance of prepared HA/PAni nanoparticles was obtained using an UV spectrophotometer (UV-1800, Shimadzu), and hydrodynamic size was measured by dynamic laser-scattering analysis (ELS-Z, Otsuka Electronics).

2.4. Measurements of light-scattering images and spectra

All scattering spectroscopic measurements and imaging were performed using an inverted microscope (Axio Observer A1, Carl Zeiss) equipped with an imaging spectrograph (Acton SP2500, Princeton Instruments) and charge-coupled device (CCD) detector (PIXIS400B, Princeton Instruments). A color CCD camera (Thorlabs, DCU224C) was also attached to the front port of the microscope to facilitate identification and alignment of single HA/PAni nanoparticles. A darkfield condenser (NA = 1.2–1.4) was used to illuminate single HA/PAni nanoparticles, and a variable aperture 40× objective (NA = 0.6–1.5) was used to collect the light scattered by single HA/PAni nanoparticles. The method for measuring the scattered spectra of single HA/PAni nanoparticles was as follows. Briefly, the spectrograph grating was placed in zero order and the spectrograph entrance slit was opened to the maximum setting to project a wide-field image onto the CCD detector. Next, HA/PAni was placed in the center of the field and the entrance slit was closed to 20 μm. Then, the spectrograph grating was rotated to disperse the first-order diffracted light onto the CCD detector. To ensure that only the scattered light from a single nanoparticle was analyzed, the region of interest was selected using the CCD control software. An adjacent empty region of the CCD detector with the same dimensions was also collected to perform background subtraction. Integration times varied, depending on lamp intensity and the scattering strength of the HA/PAni, but a typical acquisition was comprised of five exposures, each lasting 5 s. Finally, the raw scattered spectrum was normalized to correct for the lamp spectral profile, spectrograph throughput, and efficiency of the CCD detector. This process was accomplished by dividing the raw spectra by the lamp spectra, which were obtained by increasing the numerical aperture of the objective above 1.4.

2.5. Cell culture and sampling for light-scattering spectrum

All cell lines used in this study were obtained from the American Type Culture Collection. The human breast cancer cell line, MDA-MB-231, was maintained in RPMI1640 with 5% FBS; MCF-7 cells were maintained in DMEM with 10% FBS at 37 °C in 5% CO_2. To measure the scattering spectra of HA/PAni nanoparticles in the above-mentioned cells, 5×10^4 cells well^{-1} were incubated in 4-well plates with 50 μl HA/PAni (0.05 mg ml^{-1}) on a round coverslip (ϕ = 12 mm) for 4 h at 37 °C.

3. Results and discussion

Water-soluble HA/PAni polyplexes were fabricated using a nanoprecipitation method with some modifications [7]. HA was used to target CD44, which is overexpressed on the surface of invasive cancer cells and acts as a surfactant to increase the colloidal stability of HA/PAni polyplexes. On the other hand, PAni has a reversible change of its doped state as varying the environmental acidity, such as existence to EB state at neutral environments and transition to ES state at acidic environment [17–22]. To confirm this characteristic we choose two pH conditions (pH 7 and 1), which are the representative environments for existence of PAni at EB and ES states. The colloidal size of HA/PAni polyplexes was 151.9 ± 50.3 nm and 206.4 ± 64.1 nm for EB and ES HA/PAni polyplexes, respectively (figure 2(a)). We determined that these colloidal sizes are suitable for HA/PAni polyplexes acting as colorimetric probes, because it is difficult to distinguish between cell components and polyplexes in the case of a smaller size via darkfield imaging (figures S1(a)–(d)). To investigate the ability of HA/PAni polyplexes to serve as colorimetric probes by varying the doped state, the absorbance and colloidal stability of HA/PAni polyplexes were evaluated at varying pH values. At pH 1, HA/PAni polyplexes were in the doped state (ES), as indicated by the presence of the polaron bands transitions as well as π–π^* transition of the benzenoid rings at 800–1 000 nm and 400 nm of peaks, respectively (figure S1(e)) [23]. With increasing pH, the polaron bands and benzenoid rings at 800–1 000 and 400 nm gradually decreased in intensity, and a strong absorbance peak at about 720 nm was observed. The absorbance peak at 720 nm is due to excitation from the highest occupied molecular orbital of the three-ring benzenoid part of the localized quinoid ring and the two surrounding imine nitrogens in the EB state of PAni [24]. To distinguish more specifically between the EB and ES states, the absorbance ratios ($\lambda_{540}/\lambda_{450}$) were calculated at the representative wavelengths of the valley for the ES (λ_{540}) and EB (λ_{450}) states. Moreover, we also analyzed the valley of the absorbance spectrum for each pH value (figures 2(b), S1(f) and (g)), because the wavelength of the valley is correlated with the reflected light from HA/PAni polyplexes. In general, the color of objects is formed by leaving light from the surface of the objects at specific wavelength. In other words, the color of the objects can be perceived by receiving the specific reflected

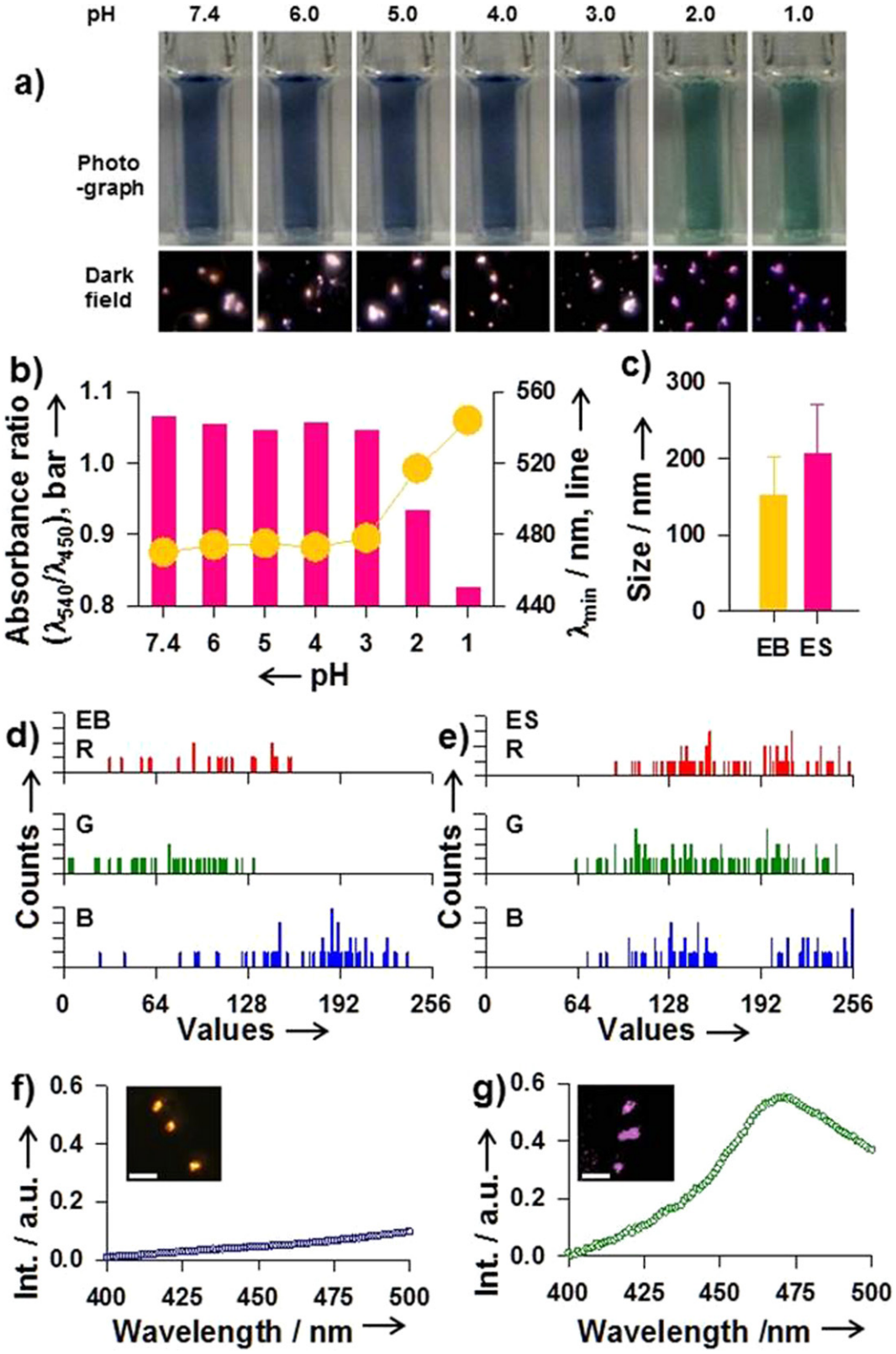

Figure 2. (a) Photographs and corresponding darkfield microscopic images for HA/PAni at the indicated pH. (b) Absorbance ratio ($\lambda_{540}/\lambda_{450}$, bar) and valley of the spectrum (λ_{min}, line and scatter) for HA/PAni at the indicated pHs. (c) Hydrodynamic diameters of EB and ES HA/PAni polyplexes. Color distributions of red (R), green (G), and blue (B) channels for (d) EB HA/PAni and (e) ES HA/PAni obtained from the original darkfield microscopic images in (d). Analysis of (f) EB HA/PAni and (g) ES HA/PAni via darkfield microscopic images (insets), and the average light-scattering spectrum ($n = 3$) for a single nanoparticle. Scale bars are 200 nm.

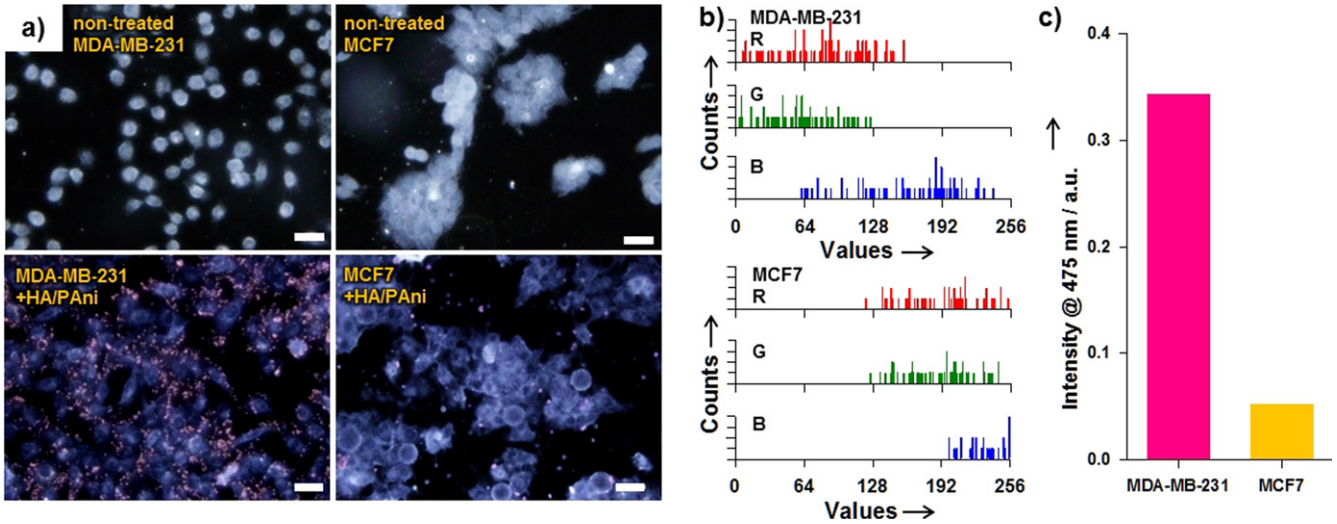

Figure 3. (a) Dark field microscopic images of MDA-MB-231 (first column) and MCF7 cells (second column) for non-treated control (first raw) and treatment of HA/PAni (second raw) conditions, respectively. All scale bars are 20 μm. (b) RGB color histograms for MCF7 (top) or MDA-MB-231 (bottom) cells treated with HA/PAni using dark field microscopic images in (a). (c) Light-scattering intensity at 475 nm obtained by NSSIA for a single HA/PAni polyplex attached on MDA-MB-231 or MCF7 cells.

wavelength of light from the objects at human naked eyes. As the wavelength of the valley is changed, the color of the HA/PAni solution also changes. As a result, HA/PAni polyplexes in the ES state (pH $<$ 3) show a green color, whereas the color of the EB state (pH $>$ 3) is blue without any aggregation or precipitation (figure 2(c)). For the sensitive detection of color changes for HA/PAni polyplexes, darkfield imaging was also conducted by varying pH values from pH 1 to pH 7.4. In the darkfield images, EB HA/PAni polyplexes exhibited a yellow color, whereas the ES HA/PAni polyplexes are shown as a pink color. As mentioned earlier, we also choose two representative pH values that existing in two different states for HA/PAni polyplexes (pH 1 and 7). To provide a quantitative assessment of the darkfield images, the RGB profiles of the images for the HA/PAni polyplexes were analyzed (figures 2(d) and (e)) [25, 26]. ES HA/PAni polyplexes had higher intensity values than EB HA/PAni polyplexes, especially in the red and green channels. Measurements of the light-scattering spectrum for single HA/PAni polyplexes were also conducted (figures 2(f) and (g)). The darkfield images show three different HA/PAni polyplexes for light-scattering spectral measurements of the EB and ES states of HA/PAni, respectively. The light-scattering spectra were measured and plotted in each state; in particular, a scattering peak was observed in the ES state at about 475 nm. From these results, we confirmed that HA/PAni polyplexes were well fabricated, and exhibited good stability and dispersion characteristics; additionally, HA/PAni also showed an ability to serve as a sensing probe to detect environmental changes, such as the surrounding pH.

To investigate the colorimetric and targeting capacity of the HA/PAni polyplexes in cancer cells, HA/PAni polyplexes were incubated with MDA-MB-231 and MCF7 cells for 4 h to observe colorimetric changes from the EB to the ES state, and the targeting ability of CD44, a biomarker expressed on the surfaces of invasive cancer cells. As shown in figure 3(a), HA/PAni polyplexes successfully acted as colorimetric probes after incubation with MDA-MB-231 cells. MDA-MB-231 cells treated with HA/PAni polyplexes exhibited a pink color in darkfield images. Furthermore, a specific interaction was observed between HA/PAni polyplexes and MDA-MB-231 cells, although HA/PAni did not show any affinity for MCF7 cells or any colorimetric changes. To further evaluate the efficiency of HA/PAni polyplexes as *in vitro* probes, the analyses of the color distribution of HA/PAni added to MDA-MB-231 and MCF7 cells were also conducted (figure 3(b)). In the case of MCF7 cells treated with HA/PAni polyplexes, the color distribution of the polyplexes exhibited a distribution analogous to the EB state, but, in the case of MDA-MB-231 cells treated with HA/PAni polyplexes, the color distribution was similar to the ES state of the HA/PAni polyplexes. The measurements of the light-scattering spectra for single HA/PAni polyplexes were also carried out (figure 3(c)). In the case of MDA-MB-231 cells treated with the HA/PAni polyplexes, the scattering intensity at 475 nm was about 0.35 between pHs 1 and 2 (figure S2). We speculate that the cause of this effect was redox biomolecules from live cancer cells that acted as a dopant. To support this argument, HA/PAni polyplexes were added to MDA-MB-231 cells for 40 h and the cells were then fixed (figure S3). HA/PAni polyplexes exhibited a pink color in darkfield images and MDA-MB-231 cells were still proliferating, even with an incubation time of 40 h. In addition, in the fixed MDA-MB-231 cells, the color of the HA/PAni polyplexes was yellow, that is, HA/PAni polyplexes did not transition to the ES state, but remained in the EB state. These results indicate that HA/PAni polyplexes have a redox-sensing potential for cancer microenvironments. During cancer cell metabolism, redox stress induced by the Warburg effect increases the concentration of redoxing molecules, such as lactic acid, pyruvic acid, co-enzymes, and biological-redoxing agents, which can act as biological dopants for the HA/PAni

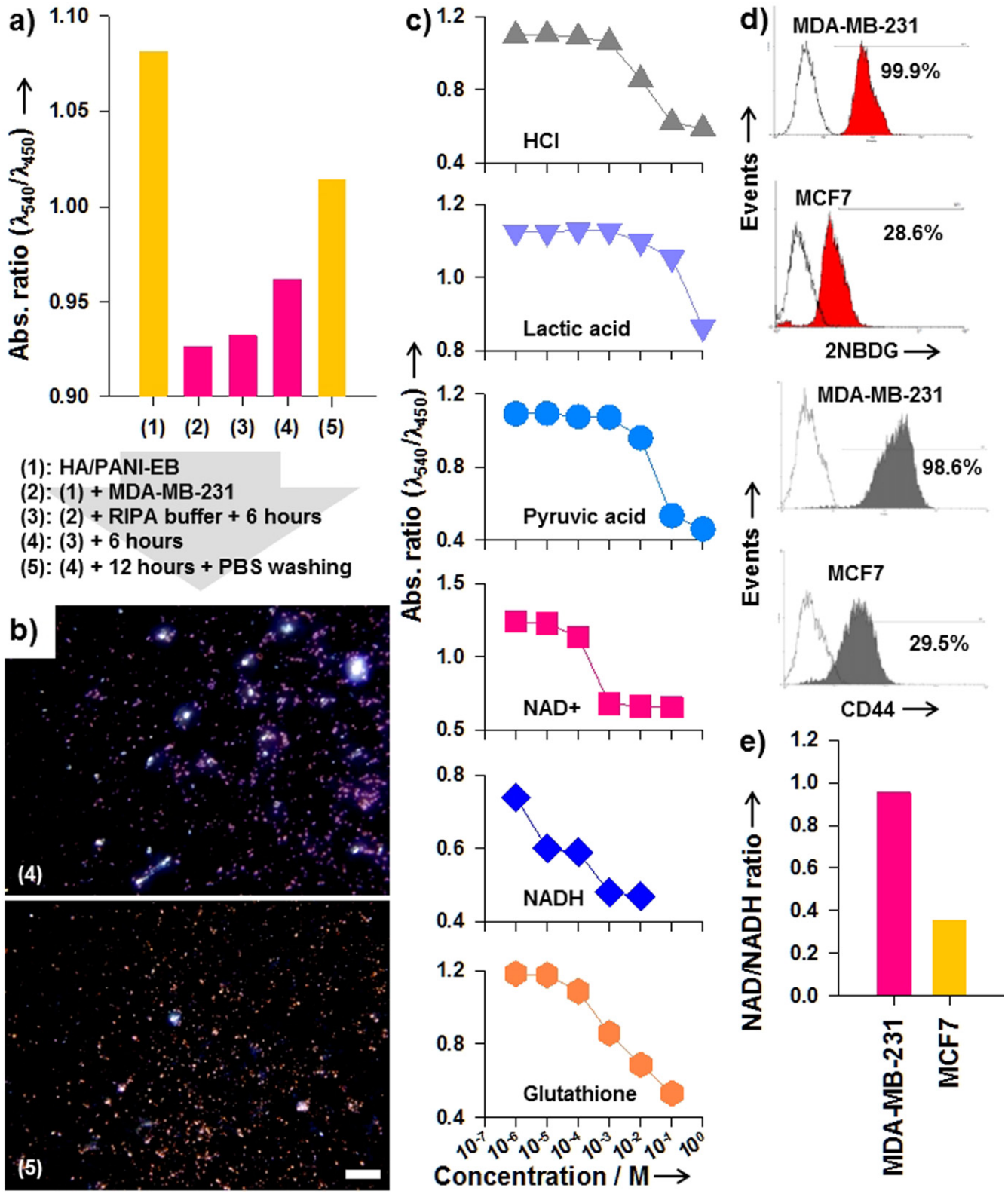

Figure 4. (a) Absorbance ratio ($\lambda_{540}/\lambda_{450}$) of HA/PAni for the indicated conditions. (b) Darkfield microscopic images corresponding to conditions for (4) and (5) in (a), respectively. (c) Absorbance ratios ($\lambda_{540}/\lambda_{450}$) of HA/PAni treated with HCl, lactic acid, pyruvic acid, NAD^+, NADH, and glutathione. (d) Flow cytometric analysis data for MDA-MB-231 and MCF7 cells for CD44. (e) NAD/NADH ratio for MDA-MB-231 and MCF7 cells.

polyplexes [27]. Thus, the confined, active coloring effect from MDA-MB-231 cells may prove to be a crucial factor in the doping and coloring of HA/PAni polyplexes. It is also known that conversion from the EB state to the ES state of PAni requires dopants [28]. Therefore, we believe that redoxing molecules generated by proliferating cancer cells act as dopants and may result in the transition of the HA/PAni polyplexes. The targeting capability of HA/PAni polyplexes toward CD44 was confirmed by dark field microscopic imaging. After the targeting, the color of HA/PAni polyplexes was changed from yellow to pink, because of redoxing molecules generated by proliferating and metastatic cancer cells, and this phenomenon can be interpreted to chemical state of HA/PAni polyplexes was transitioned from EB to ES state. We successfully observed this phenomenon at MDA-MB-231 cells, which are known as highly metastatic and stem-like cancer [29–31]. In the case of the MCF7, however, even targeting of HA/PAni polyplexes did not proceed.

For the demonstration of the doped/de-doped state reversibility of HA/PAni in biological systems, darkfield imaging and absorbance measurements were conducted under various conditions (figures 4(a), (b), and S4). As shown in figure 4(a), when HA/PAni polyplexes were incubated with MDA-MB-231 cells (2), the absorbance ratio indicated that HA/PAni polyplexes were in the ES state. After the addition of cell lysis (RIPA) buffer to MDA-MB-231 cells treated with HA/PAni (3), the absorbance ratio slightly increased but still indicated that the HA/PAni polyplexes were in the ES state. Under this condition, MDA-MB-231 cells were lysed. HA/PAni polyplexes in this condition (3) were incubated with the lysates more for 6 h (4), and the absorbance ratio indicated that the HA/PAni polyplexes were in the ES state. Moreover, the ES state of the HA/PAni polyplexes was confirmed using darkfield imaging (figure 4(b)), exhibiting a pink color after a 12 h incubation and wash step with PBS (4), The HA/PAni polyplexes were then converted into an EB-like-state (5). The absorbance ratio of HA/PAni was above 1.0, and the color of the polyplexes shifted from pink to orange. These results indicate that metabolites released from cancer cells can act as dopants for the HA/PAni polyplexes, that is, these biological-redoxing molecules can be reacted with HA/PAni polyplexes. These activated redoxing molecules are not naturally or easily removed from HA/PAni. The cell culture media did not dramatically change the pH value and did not affect the state of the HA/PAni polyplexes (figure S5). To determine the dominant biomaterial that acted as a dopant for the HA/PAni polyplexes in biological systems, doping capability was evaluated using various candidate groups, such as hydrochloric acid (HCl) as a representative dopant for PAni, lactic acid and pyruvic acid as major redoxing molecules from cancer cells for the Warburg effect [32], Nicotinamide adenine dinucleotide (NAD^+) and NADH as major biomaterials in redox reactions in biological systems [33], and glutathione as an important reducing agent in biological systems (figure 4(c)) [34]. For the conversion of the state of HA/PAni polyplexes, NAD^+ was the most sensitive material in the doping process. To verify the characteristics of the cell lines used, we confirmed glucose uptake, CD44 expression levels, and NAD/NADH ratios (figures 4(d) and (e)). 2-Deoxy-2-[(7-nitro-2,1,3-benzoxadiazol-4-yl)amino]-D-glucose (2NBDG) was used as an indicator for glucose uptake [35], which was 3.5-fold higher in MDA-MB-231 cells than in MCF7 cells. Moreover, CD44 expression levels and NAD/NADH ratios of MDA-MB-231 cells were also 3.3-fold and 2.4-fold higher, respectively, than in MCF7 cells. The hypothesis of doping procedure for HA/PAni polyplexes in cellular environments as follows. The binding toward cell surface should take precedence in order for doping of HA/PAni polyplexes because we think that proximity between HA/PAni polyplexes and cell surface is a key point for doping of HA/PAni polyplexes in cellular environment. After the binding to cell surface, we think that doping of HA/PAni polyplexes was occurred by lactic acid, pyruvic acid, which is major metabolites as well as redoxing molecules of Warburg effect [36]. This Warburg effect is known to be initiated by the glucose uptake to cells, so we preferentially confirmed glucose uptake levels for MDA-MB-231 and MCF7 cell lines using 2NBDG. Sequentially, CD44 expression levels for each cell line were also analyzed to confirm the binding affinity of HA/PAni polyplexes toward CD44. These results indicate that MDA-MB-231 cells have higher levels of glucose uptake, which can initiate the Warburg effect, a hallmark of malignant cancer cells. Thus, HA/PAni polyplexes added to MDA-MB-231 cells have a high probability to bind to and be doped with lactic acid or pyruvic acid, major redoxing molecules of the Warburg effect [37]. In addition, the high NAD/NADH ratio also potentially contributes to the doping process of the HA/PAni polyplexes in MDA-MB-231 cells.

4. Conclusions

In this research, we have fabricated HA/PAni polyplexes as active coloring probes to sense cancer redox microenvironments. We confirmed the colorimetric capability of HA/PAni polyplexes visually, measured absorbance and light-scattering spectra, and performed darkfield microscopic imaging at a single nanoparticle scale. HA/PAni polyplexes acted as colorimetric probe at various environmental pH values, concentrations of biomaterials, cancer cell lines, and cancer stages, and demonstrated a specific targeting ability to a specific cancer redox biomarker. Thus, we believe that these conjugated polyplexes represent a promising nano-platform for cancer diagnosis. Continuous attempts to optimize these conjugated polyplexes for various cancer cells and redox microenvironments of tumors would improve their specificity, selectivity, and sensitivity.

Acknowledgments

This work was supported by the National Research Foundation of Korea (NRF) funded by the Ministry of Science, ICT, and Future Planning (2015R1A2A1A05001887 and 2014R1A1A2059806).

References

[1] Hanahan D and Weinberg Robert A 2011 *Cell* **144** 646–74
[2] Sounni N E and Noel A 2013 *Clin. Chem.* **59** 85–93
[3] Friedl P and Alexander S 2011 *Cell* **147** 992–1009
[4] Schroeder A, Heller D A, Winslow M M, Dahlman J E, Pratt G W, Langer R, Jacks T and Anderson D G 2012 *Nat. Rev. Cancer* **12** 39–50
[5] Yang J *et al* 2011 *Angew. Chem., Int. Ed. Engl.* **50** 441–4
[6] Park J *et al* 2012 *Angew. Chem., Int. Ed. Engl.* **51** 945–8
[7] Choi J, Hong Y, Lee E, Kim M-H, Yoon D, Suh J, Huh Y, Haam S and Yang J 2013 *Nano Res.* **6** 356–64
[8] Zhao Y, Ji T, Wang H, Li S, Zhao Y and Nie G 2014 *J. Control. Release* **177** 11–9
[9] Heeger A J 2001 *Angew. Chem., Int. Ed Engl.* **40** 2591–611
[10] Dimitriev O P 2004 *Macromolecules* **37** 3388–95
[11] Gizdavic-Nikolaidis M, Travas-Sejdic J, Bowmaker G A, Cooney R P and Kilmartin P A 2004 *Synth. Met.* **140** 225–32
[12] Ponta H, Sherman L and Herrlich P A 2003 *Nat. Rev. Mol. Cell Biol.* **4** 33–45
[13] Götte M and Yip G W 2006 *Cancer Res.* **66** 10233–7
[14] Puré E and Cuff C A 2001 *Trends Mol. Med.* **7** 213–21
[15] Lim E-K, Kim H-O, Jang E, Park J, Lee K, Suh J-S, Huh Y-M and Haam S 2011 *Biomaterials* **32** 7941–50
[16] Park J *et al* 2013 *Integr. Biol.* **5** 669–72
[17] Varela-Álvarez A, Sordo J A and Scuseria G E 2005 *J. Am. Chem. Soc.* **127** 11318–27
[18] Hatchett D W, Josowicz M and Janata J 1999 *J. Phys. Chem.* B **103** 10992–8
[19] Kulkarni M V, Viswanath A K, Marimuthu R and Seth T 2004 *J. Polym. Sci. Polym. Chem.* **42** 2043–9
[20] Cardoso M J R, Lima M F S and Lenz D M 2007 *Mater. Res.* **10** 425–9
[21] Stejskal J, Sapurina I, Trchová M, Prokeš J, Křivka I and Tobolková E 1998 *Macromolecules* **31** 2218–22
[22] Yoo J E, Cross J L, Bucholz T L, Lee K S, Espe M P and Loo Y-L 2007 *J. Mater. Chem.* **17** 1268–75
[23] Huang W S and MacDiarmid A G 1993 *Polymer* **34** 1833–45
[24] Huang J and Kaner R B 2006 *Chem. Commun.* 367–76
[25] Bonifacio L D, Puzzo D P, Breslav S, Willey B M, McGeer A and Ozin G A 2010 *Adv. Mater.* **22** 1351–4
[26] Miranda O R, Li X, Garcia-Gonzalez L, Zhu Z-J, Yan B, Bunz U H F and Rotello V M 2011 *J. Am. Chem. Soc.* **133** 9650–3
[27] Stubbs M, McSheehy P M J, Griffiths J R and Bashford C L 2000 *Mol. Med. Today* **6** 15–9
[28] Tao S, Hong B and Kerong Z 2007 *Spectrochim. Acta* A **66** 1364–8
[29] Tu Y-F, Kaipparettu B A, Ma Y and Wong L-J C 2011 *Biochim. Biophys. Acta Bioenerg.* **1807** 1125–32
[30] Hiraga T, Ito S and Nakamura H 2011 *Oncol. Rep.* **25** 289–96
[31] Panjehpour M, Castro M and Klotz K-N 2005 *Br. J. Pharmacol.* **145** 211–8
[32] Cairns R A, Harris I S and Mak T W 2011 *Nat. Rev. Cancer* **11** 85–95
[33] Ying W 2008 *Antioxid. Redox Signal* **10** 179–206
[34] Wu G, Fang Y-Z, Yang S, Lupton J R and Turner N D 2004 *J. Nutr.* **134** 489–92
[35] Zou C, Wang Y and Shen Z 2005 *J. Biochem. Biophys. Methods* **64** 207–15
[36] Sakamoto T, Niiya D and Seiki M 2011 *J. Biol. Chem.* **286** 14691–704
[37] Kim J-W and Dang C V 2006 *Cancer Res.* **66** 8927–30